Journal of Zhejiang University-SCIENCE A (Applied Physics & Engineering) 2022 23(4):247-256
www.jzus.zju.edu.cn; www.springer.com/journal/11582
E-mail: jzus_a@zju.edu.cn

Research Article

https://doi.org/10.1631/jzus.A2100395

Seal contact performance analysis of soft seals on high-pressure hydrogen charge valves

Zhen-hao LIN[1], Long-jie YU[1], Ting-feng HUA[1], Zhi-jiang JIN[1,3], Jin-yuan QIAN[1,2]✉

[1]*Institute of Process Equipment, College of Energy Engineering, Zhejiang University, Hangzhou 310027, China*
[2]*State Key Laboratory of Fluid Power and Mechatronic Systems, Zhejiang University, Hangzhou 310027, China*
[3]*Institute of Wenzhou, Zhejiang University, Wenzhou 325036, China*

Abstract: The charge valve is an important element in the charging port of a high-pressure hydrogen storage cylinder (HP-HSC). It is normally closed after the HP-HSC is filled with hydrogen. If the seal of the charge valve is damaged, it will seriously affect the stable operation of the hydrogen supply system and may even cause safety problems. Therefore, the seal performance of the charge valve is important. In this paper, finite element analysis (FEA) is carried out to analyze the seal contact performance of hydrogenated nitrile rubber (HNBR) gaskets in the seal pair of a charge valve. The effects of different pre-compressions, seal widths, and hydrogen pressures on the seal contact performance of the charge valve are analyzed. The contact pressure on the seal surface increases with the increase of pre-compression. With a pre-compression of 2.5 mm, the maximum contact pressure without and with hydrogen pressure are 68.51 and 107.38 MPa, respectively. A contact gap appears in the inner ring of the seal surface with pre-compression below 0.15 mm. The contact gap occurs between the entire seal surface with a seal width of 1 mm. The contact pressure on the seal surface and the width of the separation area between the seal surfaces increase with the increase of the seal width. The contact gap between the seal surfaces is zero with a width of 2.5 mm. The width of the separation area between the seal surfaces decreases with the decrease of the hydrogen pressure. The width of the separation area is reduced from 0.5 mm at 35 MPa to 0.17 mm at 15 MPa. This work can be useful for improvement of the seal performance and of the design of the charge valve used in the HP-HSC.

Key words: Charge valve; Seal contact performance; High-pressure hydrogen storage cylinder (HP-HSC); Finite element analysis (FEA)

1 Introduction

With the rapid development of global industrialization, fossil fuel consumption is intensified. It is expected to increase by 56% by 2040 all over the world (Shet et al., 2021). Because fossil fuels produce large amounts of greenhouse gases during energy conversion, including carbon dioxide (CO_2) and other by-products that are harmful to the environment, the world's climate and environment have been severely damaged (Kovač et al., 2021). Therefore, to reduce the consumption of non-renewable resources such as fossil fuels and reduce the damage to the environment, it is very important to find renewable clean energy. Hydrogen gas, burning as a fuel to generate water vapor as a substance that is safe and non-toxic, is a form of renewable clean energy, which has the advantages of abundant resources, high combustion value, cleanness, and renewability, etc. Hydrogen has received extensive attention in the energy transition at the beginning of the 21st century and the hydrogen fuel cell has been widely applied (Staffell et al., 2019; Özbek et al., 2020; Peláez-Peláez et al., 2021). A major commercial application is fuel cell vehicles (Staffell et al., 2019), which benefit from refueling times of only a few minutes and ranges that are similar to those of fossil-fueled vehicles (Hong and Kim, 2018; Bai et al., 2021).

The hydrogen supply system (HSY) of a hydrogen fuel cell (HFC) vehicle is the internal energy supply system that is responsible for the storage, transportation,

✉ Jin-yuan QIAN, qianjy@zju.edu.cn
Jin-yuan QIAN, https://orcid.org/0000-0002-5438-0833

Received Aug. 17, 2021; Revision accepted Dec. 15, 2021;
Crosschecked Feb. 26, 2022; Online first Apr. 20, 2022

and use of hydrogen. It consists of a hydrogen storage device, a hydrogen supply combination valve (HSCV), and an HFC, as shown in Fig. 1. Among the hydrogen storage techniques available, high-pressure hydrogen storage cylinders (HP-HSCs) are currently widely used (Zheng et al., 2013; Li et al., 2020). They store high-pressure gaseous hydrogen at a temperature above the critical temperature. They have the advantages of low storage energy consumption, low cost, fast hydrogen charging and discharging speeds, and a wide operating temperature range. One of the important technologies for extending the range of HFC vehicles is to increase the hydrogen storage pressure and so increase the quantity of stored hydrogen. In a HFC vehicle, the hydrogen is usually reserved in an HP-HSC at 35 or 70 MPa (Cheng et al., 2017). However, the hydrogen fed into the fuel cell must be a low-pressure gas at 0.1–0.3 MPa (Abderezzak et al., 2017; Lin et al., 2018). Therefore, an HSCV is required to decompress the high-pressure hydrogen in the HP-HSC and then stably release it into the fuel cell. In the working conditions of high temperature, large pressure difference, and high purity hydrogen, the requirements for the performance of the HSCV in terms of sealing, decompression, and safety are increasing. An HSCV is mainly composed of three parts: the pressure and temperature sensors, the multi-function combined valve (MFCV) (Chen et al., 2019; Qian et al., 2019), and the charge valve. The hydrogen in the hydrogen fueling station (HFS) is stored in an HP-HSC through the charge valve. The high-pressure hydrogen achieves flow restriction and pressure reduction through the MFCV. After the HP-HSC has discharged hydrogen, the charge valve will be closed for a long time and will not be opened until the next charging. Therefore, the seal performance of the charge valve is particularly important in HSY.

In recent years, with the rapid development of computer-aided engineering, finite element analysis (FEA) shows high efficiency and cost savings. Thus, it is widely adopted for studying the seal performance of seal pairs in engineering. Romanik et al. (2019) studied the contact stress of the seal contact surface between ball and seat by FEA. The accuracy of the FEA results was verified by experiments. Dev et al. (2016) verified the stress-strain states in the seal pair of the gas lift valve under different pressures and predicted the seal contact pressure. Gorash et al. (2016)

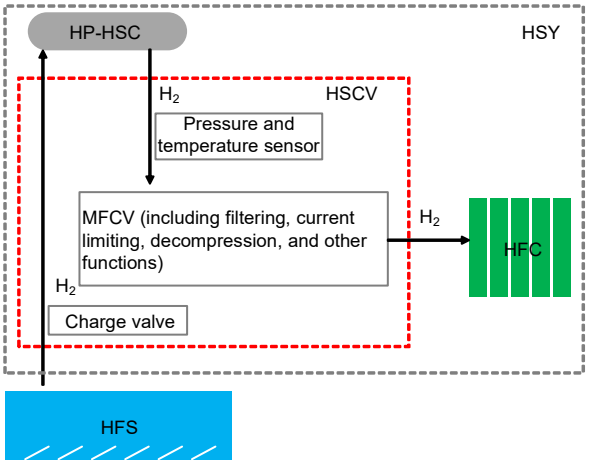

Fig. 1 Hydrogen supply process for hydrogen fuel cell vehicles

conducted a numerical study on the deformation of the metal seal contact surface of the relief valve with different geometric shapes. Wu et al. (2010) carried out an FEA on the contact stress of the contact surface between the valve poppet and the seat with two seal models of high-pressure cone valve, and the FEA results agreed well with experimental results. Kan and Ding (2016) analyzed the influence of changes in bias parameters on seal performance of a double offset butterfly valve. Kwak et al. (2019) conducted an FEA on the effect of laminated seal shape on contact pressure of a seal pair in a butterfly valve. In general, with the help of FEA software, research on the seal performance of the seal pair has been widely used for valves.

Compared with metal hard seals, non-metallic soft seals are easier to process and require less seal force. At the same time, with the continuous development of new technologies and non-metallic materials, non-metallic soft seals are increasingly widely used as seals in various mechanical fields. Modified polytetrafluoroethylene (PTFE) was used in the soft seal between the core and seat of the ball valve (Ben Jemaa et al., 2012; Romanik et al., 2019). Modified polyetheretherketone (PEEK) was adopted to seal the gas in the valve or compressor in a deep-sea environment (Wu et al., 2010; Nie et al., 2021). In the FEA, the non-metallic materials used in the soft seal are hyperplastic, and their complex material nonlinearity and geometric nonlinearity need to be considered. Song et al. (2009) numerically calculated the contact performance of the ball valve seal pair with nitrile rubber (NBR) based on the Mooney-Rivlin method. Lin et al.

(2020) studied the deformation of a polydimethylsiloxane (PDMS) membrane in a microfluidic passive valve via fluid-structure interaction. Jayanath et al. (2016) studied the contact stress of the NBR seal ring on a valve by FEA, and the experimental results were consistent with the FEA results.

In this paper, a non-metallic soft seal structure of a charge valve of the HP-HSC is designed. FEA is carried out to analyze the contact performance of hydrogenated nitrile rubber (HNBR) gaskets in the seal pair of charge valves. The influence of different pre-compressions, seal widths, and hydrogen pressures on the contact performance is compared. This work can be useful for the improvement of the seal and the design of the charge valve used in the HP-HSC.

2 FEA model

2.1 Geometry model

The structure of the charge valve as shown in Fig. 2, mainly consists of bonnet, stem, plug, seal gasket, and body. In Fig. 2, F is the pre-tightening force; p_1 is the hydrogen pressure; D_i and D_o are the inner and outer diameters of the contact surface between the plug and body, respectively; b is the width of the seal surface. When HP-HSC is full of hydrogen, the hydrogen filling is stopped. The research focuses on the seal behavior such as leakage prevention in the contact area between the gasket and the seal surface of the valve body, so the charge valve is greatly simplified. Only the plug, gasket, and body remain.

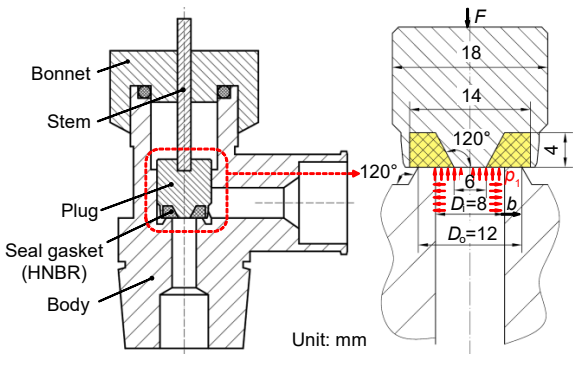

Fig. 2 Structure of the charge valve

2.2 Boundary conditions and grid independence

The model of the charge valve is simplified before the FEA, as shown in Fig. 3. The parts that have little effect on the seal analysis of the seal pair are ignored, only the plug, gasket, and body remain. Due to the symmetry of the charge valve structure, half of the model is analyzed. The plug and body are made of stainless steel, which is set as rigid in the FEA. The body is set as fixed. The symmetry plane of the model is set as frictionless support. The pre-compression is loaded on the upper end surface of the plug in a remote displacement manner along the negative direction of the y-axis. The pre-compression (s) range is 0.05–0.25 mm. The surface of the seal gasket in contact with hydrogen is constrained by the inner pressure. The pressure (p_1) range is 15–35 MPa. The nonlinear connection analysis model is used to calculate the contact problem. The contact between the plug and seal gasket is set as bonded, and the contact between the seal gasket and the body uses frictional behavior with a friction coefficient of 0.01. In the FEA, two steps of loading are carried out. The first step is to load the pre-compression and the second step is to load the hydrogen pressure.

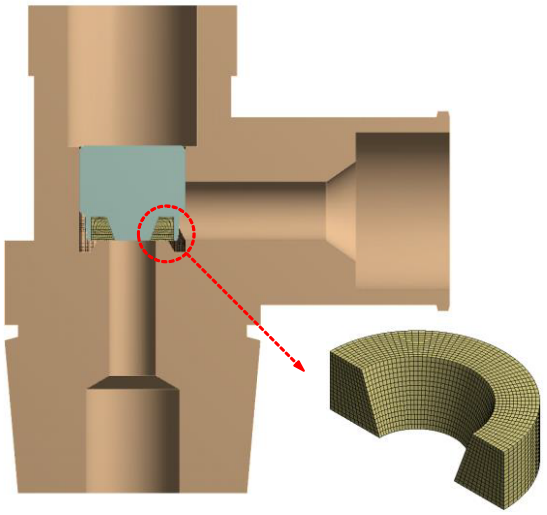

Fig. 3 Numerical model and mesh

The seal gasket is made of HNBR. This kind of material exhibits complex material and geometric nonlinearity. It is usually assumed that the rubber material is hyperplastic and that the volume remains unchanged after deformation. The Mooney-Rivlin method is widely used in FEA to describe the strain energy function of rubber materials (Zhou et al., 2018). In this paper, Poisson's ratio of HNBR is 0.499, and the two-parameter method is used in the material performance setting

(Marckmann and Verron, 2006). The strain energy density function is expressed as

$$W=C_{10}\left(I_1-3\right)+C_{01}\left(I_2-3\right), \tag{1}$$

where W refers to the strain energy density, I_1 and I_2 are the first and second strain tensor invariants, respectively, and C_{10} and C_{01} are the Mooney-Rivlin coefficients. Material properties of HNBR are 2.77 MPa (C_{10}) and 1.44 MPa (C_{01}), respectively. The fitting curves are shown in Fig. 4.

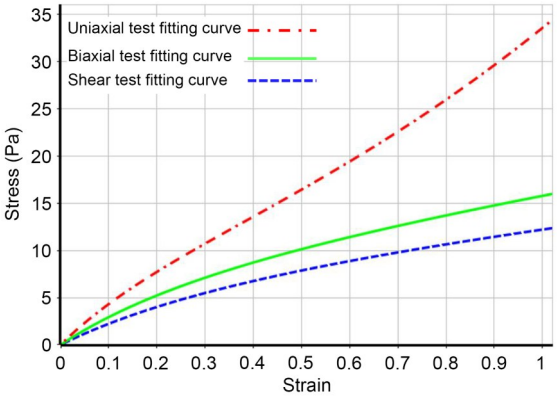

Fig. 4 Fitting curves of the HNBR material property in FEA

The quality of the grid has an important influence on the accuracy of the numerical model. The ANSYS Workbench Mesh platform is used for grid generation. The seal gasket adopts structural grid division (Solid 186), as shown in Fig. 3. To eliminate the influence of the number of grid elements on the calculation results, it is necessary to verify the independence of the grids before performing the finite element calculations. The numbers of grid elements are 5537, 10271, 21013, 40457, and 62853, respectively, which are getting from changing the element size. The average and maximum contact pressures of the contact surface between plug and body are selected as the investigated parameters, as shown in Fig. 5. It is indicated that when the number of grid elements is greater than 21013, the deviations are within 3.0% and 6.5%, respectively. Therefore, the grid independence has been verified within the scope of the survey. More grids mean more accurate simulation results, but more resources are consumed. Therefore, to obtain the optimal mesh quality and computational efficiency, a mesh method of about 21013 elements is selected.

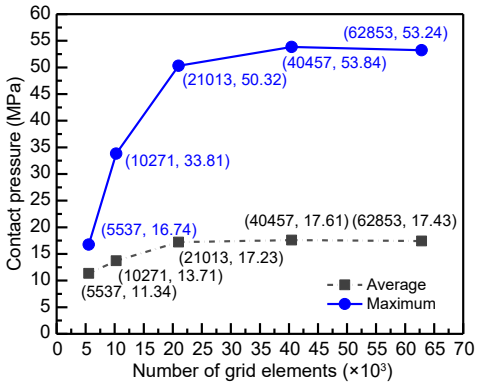

Fig. 5 Contact pressure with different number of grid elements

2.3 Method validation

To validate the accuracy of numerical methods and simulation results, a comparison with theoretical calculation and similar simulation is conducted.

A comparison with the results of theoretical calculation is conducted first. According to the force diagram in Fig. 2, the theoretical average stress P_T on the contact surface between the plug and body can be obtained:

$$P_T=\frac{F-\frac{p_1\pi D_i^2}{4}}{\frac{\pi\left(D_o^2-D_i^2\right)}{4}}. \tag{2}$$

In the method validation process, assuming that no hydrogen pressure is applied, the other boundary conditions are the same as those in Section 3.1. Pre-tightening forces of 1000, 2000, and 3000 N are selected. The average stress P_F on the contact surface between the plug and body is extracted in FEA. Theoretical calculation results and FEA results of average stress are shown in Table 1. It can be seen from Table 1 that the maximum deviation is 2.9%. Therefore, the deviation between the theoretical calculation results and the FEA results is very small, which verifies that the FEA results are reliable.

Then a comparison with similar simulations is conducted. Cao et al. (2019) studied the dynamic and

Table 1 Theoretical and FEA results of average stress

F (N)	P_T (MPa)	P_F (MPa)	Deviation (%)
1000	15.92	15.98	<1
2000	31.85	31.88	<1
3000	47.77	49.16	2.9

static seal performance of the elastic check valve spool by FEA. In the main parts of their paper, the valve spool was made of rubber material, the Mooney-Rivlin two-parameter method was selected as the constitutive model, and the plug was modeled with a displacement boundary condition. Similarly, the same method is adopted in this paper. Although this paper pays attention to the seal contact performance of a seal gasket and not a valve spool, Cao et al. (2019)'s study can indirectly validate the accuracy of the simulation results.

3 Results and discussion

3.1 Effects of pre-compression on contact performance

To analyze the effect of different pre-compressions on the contact performance of the charge valve, five pre-compressions (s=0.05, 0.10, 0.15, 0.20, and 0.25 mm, with compression percentages relative to the thickness of the gasket of 1.25%, 2.50%, 3.75%, 5.00%, and 6.25%, respectively) are selected to study the contact pressure and gap of the seal surface between plug and body. The width of the seal surface (b) used in this section is 2.0 mm. The contact pressure of the seal surface without hydrogen pressure is studied first. It can be seen from Figs. 6a and 6e that the contact pressure on the seal surface is uniformly distributed along the circumferential direction while, along the radial direction, it shows a trend of low in the middle and high on both sides. The curve distribution of contact pressure is U-shaped. Under the pre-compression, the seal gasket in contact with the body is squeezed inward, while the other part that is not in contact with the body moves in the negative direction of the y-axis. Therefore, a structural discontinuity is formed on the contact surface of the seal gasket at the contact and non-contact interfaces, that is, the locations of the diameter R_x=4 and 6 mm. It can be seen from Fig. 6e that the contact pressure on the seal surface increases with the increase of pre-compression, showing a linear increase trend at the same position. When the pre-compression reaches 0.25 mm, the maximum contact pressure on the seal surface is 68.51 MPa and it appears at R_x=6 mm.

After the HP-HSC is filled with hydrogen, the pressure reaches 35 MPa. Therefore, the seal performance of the seal pair of the charge valve under the

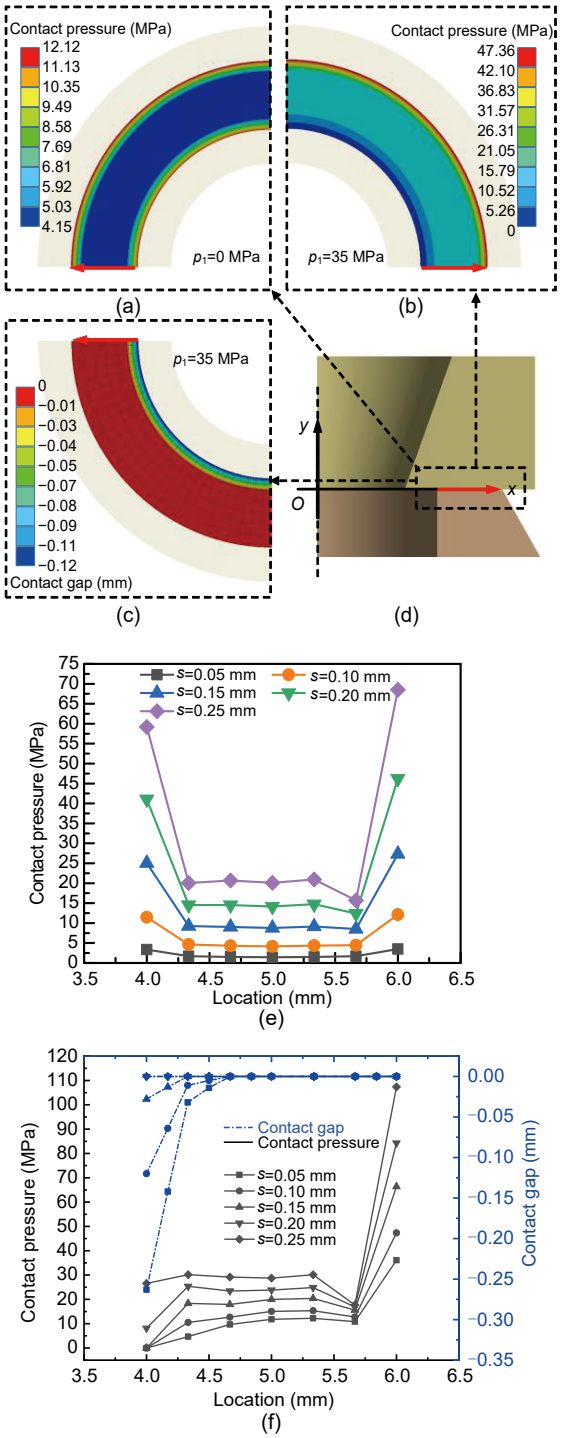

Fig. 6 Contact performance on seal surface: (a) contact pressure with p_1=0, s=0.10 mm, and b=2.0 mm; (b) contact pressure with p_1=35 MPa, s=0.10 mm, and b=2.0 mm; (c) contact gap with p_1=35 MPa, s=0.10 mm, and b=2.0 mm; (d) schematic diagram of data extraction on seal surface; (e) curves of contact pressure along x-axis with different pre-compressions at p_1=0 and b=2.0 mm; (f) curves of contact pressure and gap along x-axis with different pre-compressions at p_1=35 MPa and b=2.0 mm

action of high-pressure hydrogen is particularly important. It can be seen from Fig. 6b that the contact pressure on the seal surface is uniformly distributed along the circumferential direction, while it increases with the increase of the radius of R_x along the radial direction. Compared with the case of no hydrogen pressure, the contact pressure at R_x=4 mm is significantly lower than that at R_x=6 mm with a hydrogen pressure of 35 MPa. This is because the inner ring area of the seal surface is compressed in the positive direction of the y-axis under the action of hydrogen pressure. The contact gap represents the change in the gap between the two pairs of contact surfaces. A gap value less than zero indicates that the two pairs of contact surfaces are separated. The gap value of zero means that the two pairs of contact surfaces do not separate. When the pre-compression is less than the compression of the hydrogen pressure, the separation phenomenon of the seal surface between the plug and body occurs, as shown in Fig. 6c where the contact gap occurs. At the same time, the contact pressure in these areas is zero, as shown in Fig. 6f. When the pre-compression is 0.1 mm, the absolute value of the maximum contact gap reaches 0.12 mm. As the R_x increases, the contact gap gradually approaches zero and the end of the separation of the seal surface is at R_x=4.67 mm. This is because the area remote from the hydrogen pressure is less affected by that high pressure but is more affected by the pre-compression. However, with the increase of the pre-compression, the contact pressure on the seal surface increases. When the pre-compression reaches 0.25 mm, the maximum contact pressure on the seal surface is 107.38 MPa, and it appears where R_x=6 mm. When the pre-compression is greater than 0.15 mm, the contact pressure at R_x=4 mm is greater than zero. If the contact gap is less than zero the seal surface is separated; if it is equal to zero then the seal surface is not separated. In summary, although increasing the pre-compression can effectively inhibit the separation between the seal surfaces, excessive pre-compression brings greater contact pressure, which may lead to failure of the seal surfaces. Therefore, it is necessary to determine the appropriate pre-compression.

To explore the seal process of the seal gasket under the combined action of pre-compression and hydrogen pressure, the variation of contact pressure with loading time was analyzed. The pre-compression is loaded at 0–1 s, and the hydrogen pressure is loaded at 1–2 s. The analysis result is shown in Fig. 7. The curve in Fig. 7 has an inflection point at 1 s, and the trend of the contact pressure changes after 1 s. For the inner ring of the seal surface, the contact pressure gradually increases with time under the action of pre-compression, and then the contact pressure gradually decreases until it reaches a stable value after the loading of hydrogen pressure is added, as shown in Fig. 7b. This is because the downward compression by the pre-compression and the upward compression by the hydrogen pressure work synergistically after 1 s. The stable contact pressure on the inner ring of the seal surface is lower than the hydrogen pressure, which indicates the seal stress is less than the hydrogen pressure, and the location has not reached the precondition for seal. For the outer inner ring of the seal surface, the contact pressure gradually increases throughout the loading process. This is because the area far away from the hydrogen pressure is less affected by the hydrogen pressure. However, the contact pressure continues to

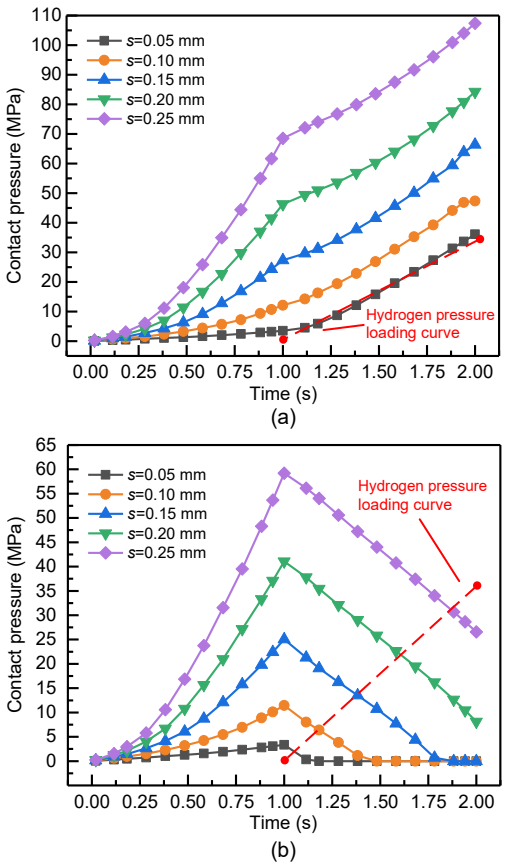

Fig. 7 Variation of contact pressure with time (b=2.0 mm and p_1=35 MPa): (a) outer ring of seal surface (R_x=6 mm); (b) inner ring of seal surface (R_x=4 mm)

increase after 1 s, because the non-metallic seal gasket is squeezed and expanded to the outer ring. The contact pressure curve is above the hydrogen pressure loading curve, which indicates that the seal stress is greater than the hydrogen pressure and the location has reached the precondition for the seal.

3.2 Effects of seal width on contact performance

To analyze the effect of different seal widths on the contact performance of the charge valve, four seal widths (b=1.0, 1.5, 2.0, and 2.5 mm) are selected for studying the contact pressure and the gap of seal surface between plug and body. The pre-compression is 0.10 mm and the hydrogen pressure is 35 MPa. The contact pressure and gap distribution along the x-axis with the four seal widths are shown in Fig. 8. When the seal width is 1.0 mm, the maximum contact pressure appears in the middle area of the seal surface, and the inner and outer rings of seal surface are both zero. The maximum contact pressure is 13.97 MPa. However, due to the small seal width, the hydrogen pressure has a greater impact on the contact pressure distribution, which leads to a separation between the seal surfaces. The maximum absolute value of the contact gap is 0.297 mm, which appears at R_x=4 mm. The minimum absolute value of the contact gap is 0.016 mm, which appears at R_x=4.67 mm. Therefore, the seal width is too small to achieve the conditions for a seal. However, with the increase of the seal width, the contact pressure on the seal surface increases, especially, the contact pressure on the outer ring is more obvious. At the same time, it can be found from Fig. 8a that, as the seal width increases, the separation location between the seal surfaces decreases. When the seal width reaches 2.5 mm, the contact gap between the seal surfaces disappears. However, the contact pressure is small at R_x=4 mm, and the conditions for forming a seal cannot be achieved. When the seal width is greater than 1.5 mm, the contact pressure on the seal surface along the radial direction tends to increase. Therefore, a reasonable increase in the seal width is beneficial for improving the seal performance of the charge valve.

The variation of contact pressure with loading time is shown in Fig. 9. Under the action of the pre-compression alone, the contact pressure on the inner and outer rings of the seal surface increases with the increase of the loading time, and its growth rate also

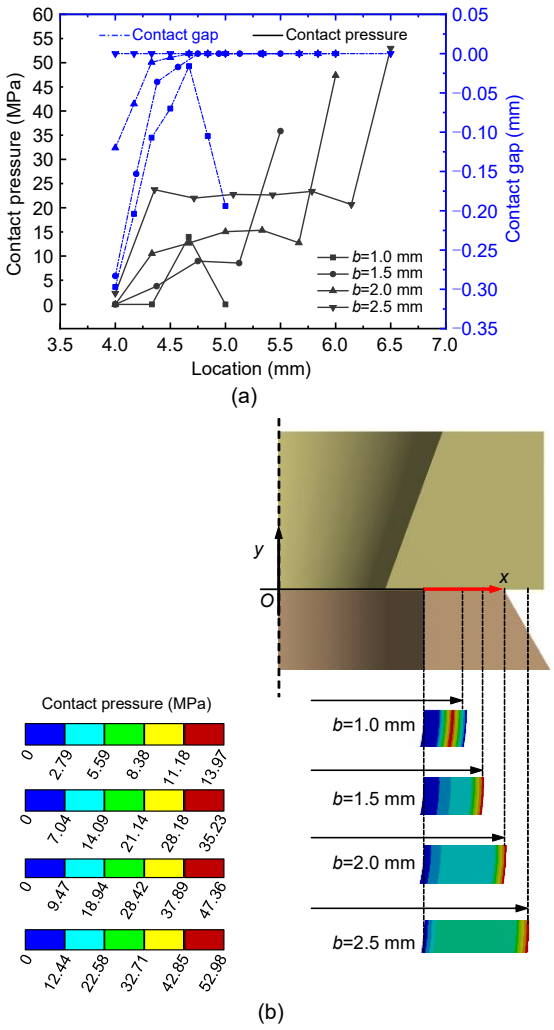

Fig. 8 Contact pressure and gap distribution along the x-axis with different seal widths at p_1=35 MPa and s=0.10 mm: (a) contact pressure and gap curves; (b) contact pressure cloud pictures

increases. However, under the synergistic effect of both pre-compression and hydrogen pressure, the contact pressure of the inner ring gradually decreases to a stable value. When the seal width is less than 2.5 mm, the contact pressure is zero. Combined with Fig. 8b, the area where the contact pressure on the seal surface does not increase as the seal width decreases can be found. The stable value on the inner ring of the seal surface is lower than the hydrogen pressure and, therefore, this location has not reached the precondition for sealing. For the outer ring of the seal surface, after the hydrogen pressure is loaded, the contact stress still increases with the increase of the loading time, except for the case where the seal width is 1.0 mm. Therefore, it can be seen from Fig. 9a that, when the width is

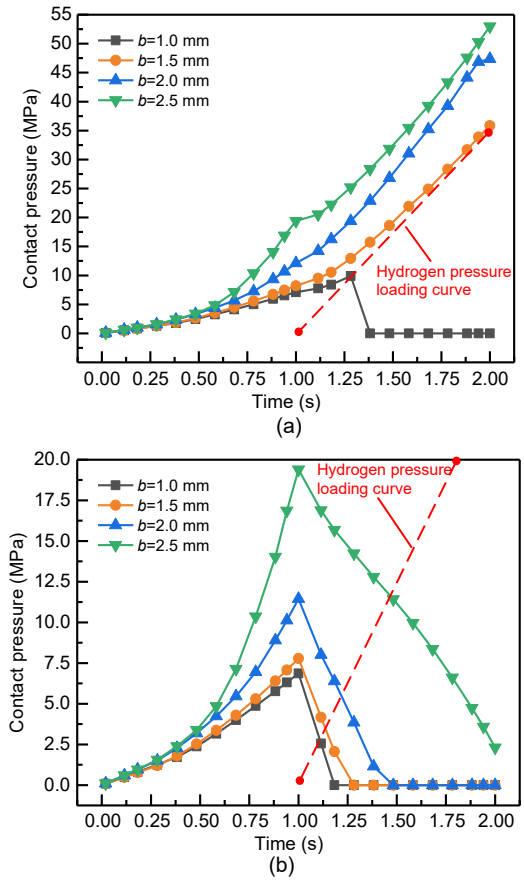

Fig. 9 Variation of contact pressure with time (s=0.1 mm and p_1=35 MPa): (a) outer ring of seal surface; (b) inner ring of seal surface (R_x=4 mm)

greater than 1.5 mm, the outer ring has reached the precondition for sealing.

3.3 Effects of hydrogen pressure on contact performance

As the hydrogen in the HP-HSC is slowly consumed to provide energy for the vehicle, the pressure in the HP-HSC gradually decreases. Five hydrogen pressures (p_1=15, 20, 25, 30, and 35 MPa) are, therefore, selected to study the contact pressure and gap of the seal surface between plug and body. The precompression is 0.10 mm and the seal width is 2.0 mm. The von Mises stress with time, at five hydrogen pressures, is shown in Fig. 10. It can be seen from Fig. 10 that, when the loading hydrogen pressures are 15, 20, 25, 30, and 35 MPa, the maximum von Mises stresses are 6.72, 9.86, 12.74, 15.64, and 18.62 MPa, respectively. With the increase of hydrogen pressure, the increment of von Mises stresses decreases. The contact pressure and gap distribution along the x-axis with the five hydrogen pressures are shown in Fig. 11. It can be seen from Fig. 11 that the contact pressure on the seal surface under the five hydrogen pressures shows an increasing trend along the positive direction of the x-axis. Similarly, the contact gap on the seal surface increases to zero along the positive x-axis. With the decrease of the hydrogen pressure, the contact pressure on the seal surface decreases. Similarly, as the hydrogen pressure decreases, the contact gap at R_x=4 mm decreases. When the hydrogen pressure is 35 MPa, the width of the separation area between the seal surfaces is 0.5 mm. When the hydrogen pressure is reduced to 15 MPa, the width of the separation area between the seal surfaces is 0.17 mm. Therefore, it can be seen that as the hydrogen in the HP-HSC decreases,

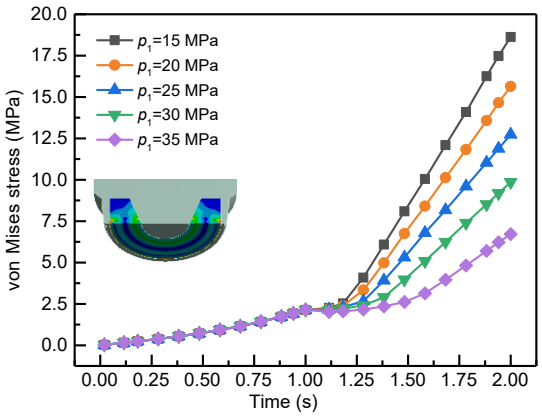

Fig. 10 von Mises stresses of seal gasket with different hydrogen pressures at b=2.0 mm and s=0.10 mm

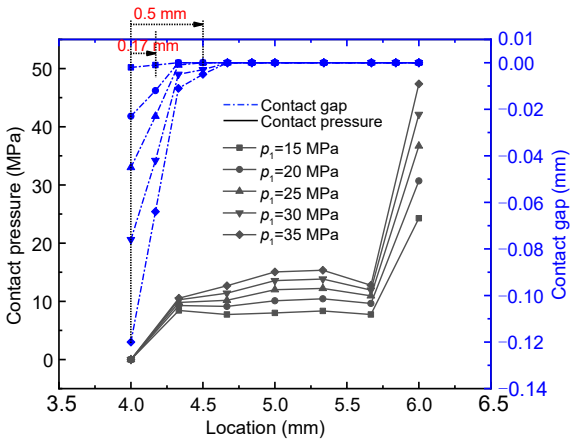

Fig. 11 Contact pressure and gap distribution along the x-axis with different hydrogen pressures at b=2.0 mm and s=0.10 mm

the impact on the seal surface of the charge valve decreases.

4 Conclusions

In this paper, a non-metallic soft seal structure of a charge valve for the HP-HSC is designed. FEA is carried out to analyze the contact performance of HNBR gaskets in the seal pair of charge valves. Firstly, the effect of different pre-compressions on the contact performance of the charge valve is analyzed. The contact pressure on the seal surface increases with the increase of pre-compression. When the pre-compression is 2.5 mm, the maximum contact pressures without and with a hydrogen pressure of 35 MPa are 68.51 and 107.38 MPa, respectively. When the pre-compression is less than 0.15 mm, the contact gap appears in the inner ring of the seal surface. Secondly, the effect of different seal widths on the contact performance of the charge valve is analyzed. When the seal width is 1.0 mm, a contact gap occurs between the entire seal surface. As the seal width increases, the contact pressure on the seal surface and the width of the separation area between the seal surfaces also increase. When the width is 2.5 mm, the contact gap between the seal surfaces is zero. Finally, the effect of different hydrogen pressures on the contact performance of the charge valve is analyzed. The width of the separation area between the seal surfaces decreases with the decrease in the hydrogen pressure. When the hydrogen pressure is 35 MPa, the width of the separation area between the seal surfaces is 0.5 mm. When the hydrogen pressure is reduced to 15 MPa, the width of the separation area between the seal surfaces is 0.17 mm.

Acknowledgments

This work is supported by the National Natural Science Foundation of China (No. 52175067), the Science and Technology Department of Zhejiang Province (No. 2021C01021), China, and the Young Elite Scientist Sponsorship Program by China Association for Science and Technology (No. YESS20200154).

Author contributions

Zhen-hao LIN and Jin-yuan QIAN designed the research. Zhen-hao LIN, Long-jie YU, and Ting-feng HUA processed the corresponding data. Zhen-hao LIN wrote the first draft of the manuscript. Long-jie YU and Ting-feng HUA helped to organize the manuscript. Zhi-jiang JIN and Jin-yuan QIAN revised and edited the final version.

Conflict of interest

Zhen-hao LIN, Long-jie YU, Ting-feng HUA, Zhi-jiang JIN, and Jin-yuan QIAN declare that they have no conflict of interest.

References

Abderezzak B, Busawon K, Binns R, 2017. Flows consumption assessment study for fuel cell vehicles: towards a popularization of FCVs technology. *International Journal of Hydrogen Energy*, 42(17):12905-12911. https://doi.org/10.1016/j.ijhydene.2016.12.152

Bai YF, Zhang CZ, Duan H, et al., 2021. Modeling and optimal control of fast filling process of hydrogen to fuel cell vehicle. *Journal of Energy Storage*, 35:102306. https://doi.org/10.1016/j.est.2021.102306

Ben Jemaa MC, Mnif R, Fehri K, et al., 2012. Design of a new tribometer for tribological and viscoelasticity studies of PTFE valve seats. *Tribology Letters*, 45(1):177-184.

Cao C, Zhao JY, Li GL, et al., 2019. Dynamic and static sealing performance of elastic check valve spool. *The Journal of Engineering*, 2019(13):28-31. https://doi.org/10.1049/joe.2018.8979

Chen FQ, Ren XD, Hu B, et al., 2019. Parametric analysis on multi-stage high pressure reducing valve for hydrogen decompression. *International Journal of Hydrogen Energy*, 44(59):31263-31274. https://doi.org/10.1016/j.ijhydene.2019.10.004

Cheng J, Xiao JS, Bénard P, et al., 2017. Estimation of final hydrogen temperatures during refueling 35 MPa and 70 MPa tanks. *Energy Procedia*, 105:1363-1369. https://doi.org/10.1016/j.egypro.2017.03.505

Dev B, Samudrala O, Wang JF, 2016. Characterization of leak rates in thermoplastic barrier valve seals under high static and cyclic pressure loads. *Journal of Petroleum Science and Engineering*, 145:279-289. https://doi.org/10.1016/j.petrol.2016.05.016

Gorash Y, Dempster W, Nicholls WD, et al., 2016. Study of mechanical aspects of leak tightness in a pressure relief valve using advanced FE-analysis. *Journal of Loss Prevention in the Process Industries*, 43:61-74. https://doi.org/10.1016/j.jlp.2016.04.009

Hong BK, Kim SH, 2018. (Invited) recent advances in fuel cell electric vehicle technologies of Hyundai. *ECS Transactions*, 86(13):3-11. https://doi.org/10.1149/08613.0003ecst

Jayanath S, Achuthan A, Mashue A, et al., 2016. A subscale experimental test method to characterize extrusion-based elastomer seals. *Journal of Tribology*, 138(3):032201. https://doi.org/10.1115/1.4032175

Kan BA, Ding JN, 2016. Criterion for non-interference of solid metal seal pair in double-offset butterfly valve. *Journal of the Brazilian Society of Mechanical Sciences and Engineering*, 38(6):1745-1752.

https://doi.org/10.1007/s40430-016-0544-4

Kovač A, Paranos M, Marciuš D, 2021. Hydrogen in energy transition: a review. *International Journal of Hydrogen Energy*, 46(16):10016-10035.

Kwak HS, Seong H, Kim C, 2019. Design of laminated seal in cryogenic triple-offset butterfly valve used in LNG marine engine. *International Journal of Precision Engineering and Manufacturing*, 20(2):243-253. https://doi.org/10.1007/s12541-019-00056-6

Li JQ, Myoung NS, Kwon JT, et al., 2020. A theoretical analysis of temperature rise of hydrogen in high-pressure storage cylinder during fast filling process. *Advances in Mechanical Engineering*, 12(12). https://doi.org/10.1177/1687814020971920

Lin ZH, Ou SQ, Elgowainy A, et al., 2018. A method for determining the optimal delivered hydrogen pressure for fuel cell electric vehicles. *Applied Energy*, 216:183-194. https://doi.org/10.1016/j.apenergy.2018.02.041

Lin ZH, Li XJ, Jin ZJ, et al., 2020. Fluid-structure interaction analysis on membrane behavior of a microfluidic passive valve. *Membranes*, 10(10):300. https://doi.org/10.3390/membranes10100300

Marckmann G, Verron E, 2006. Comparison of hyperelastic models for rubber-like materials. *Rubber Chemistry and Technology*, 79(5):835-858. https://doi.org/Doi 10.5254/1.3547969

Nie SL, Guo M, Yin FL, et al., 2021. Research on fluid-structure interaction for piston/cylinder tribopair of seawater hydraulic axial piston pump in deep-sea environment. *Ocean Engineering*, 219:108222. https://doi.org/10.1016/j.oceaneng.2020.108222

Özbek E, Yalin G, Ekici S, et al., 2020. Evaluation of design methodology, limitations, and iterations of a hydrogen fuelled hybrid fuel cell mini UAV. *Energy*, 213:118757. https://doi.org/10.1016/j.energy.2020.118757

Peláez-Peláez S, Colmenar-Santos A, Pérez-Molina C, et al., 2021. Techno-economic analysis of a heat and power combination system based on hybrid photovoltaic-fuel cell systems using hydrogen as an energy vector. *Energy*, 224:120110. https://doi.org/10.1016/j.energy.2021.120110

Qian JY, Chen MR, Gao ZX, et al., 2019. Mach number and energy loss analysis inside multi-stage tesla valves for hydrogen decompression. *Energy*, 179:647-654. https://doi.org/10.1016/j.energy.2019.05.064

Romanik G, Jaszak P, Rogula J, 2019. Cooperation of the PTFE sealing ring with the steel ball of the valve subjected to durability test. *Open Engineering*, 9(1):321-328. https://doi.org/10.1515/eng-2019-0028

Shet SP, Priya SS, Sudhakar K, et al., 2021. A review on current trends in potential use of metal-organic framework for hydrogen storage. *International Journal of Hydrogen Energy*, 46(21):11782-11803. https://doi.org/10.1016/j.ijhydene.2021.01.020

Song XG, Wang L, Park YC, 2009. Analysis and optimization of nitrile butadiene rubber sealing mechanism of ball valve. *Transactions of Nonferrous Metals Society of China*, 19(S1): S220-S224. https://doi.org/10.1016/S1003-6326(10)60274-9

Staffell I, Scamman D, Abad AV, et al., 2019. The role of hydrogen and fuel cells in the global energy system. *Energy & Environmental Science*, 12(2):463-491. https://doi.org/10.1039/C8EE01157E

Wu SJ, Yang CJ, Chen Y, et al., 2010. A study of the sealing performance of a new high-pressure cone valve for deep-sea gas-tight water samplers. *Journal of Pressure Vessel Technology*, 132(4):041601. https://doi.org/10.1115/1.4001204

Zheng CX, Wang L, Li R, et al., 2013. Fatigue test of carbon epoxy composite high pressure hydrogen storage vessel under hydrogen environment. *Journal of Zhejiang University-SCIENCE A (Applied Physics & Engineering)*, 14(6):393-400. https://doi.org/10.1631/jzus.A1200297

Zhou CL, Chen GH, Liu PF, 2018. Finite element analysis of sealing performance of rubber D-ring seal in high-pressure hydrogen storage vessel. *Journal of Failure Analysis and Prevention*, 18(4):846-855. https://doi.org/10.1007/s11668-018-0472-y